(Received 4 August 2024, Accepted 19 September 2024, Scheduled 23 September 2024)

Topology-Optimized Plasmonic Nanoantenna for Efficient Single-photon Extraction

Min Chen[1,2,#], Lian Shen[1,2,#], Yifei Hua[1,2], Zijian Qin[1,2], and Huaping Wang[1,*]

[1] *Ocean College, ZJU-Hangzhou Global Science and Technology Innovation Center*
Key Laboratory of Ocean Observation Imaging Testbed of Zhejiang Province, Zhejiang University, Hangzhou 310058, China
[2] *Interdisciplinary Center for Quantum Information, State Key Laboratory of Modern Optical Instrumentation*
College of Information Science and Electronic Engineering, Zhejiang University, Hangzhou 310027, China

ABSTRACT: Quantum emitters coupled to plasmonic nanostructures can act as extremely bright single-photon sources. Interestingly, the mode volumes supported by the plasmonic nanostructures can be several orders of magnitude smaller than the cubic wavelength, which leads to dramatically enhanced light-matter interactions and drastically increased photon emission. However, the requirements of a small mode volume for emission speed-up are always contradictory with a sufficiently large mode volume for efficient extraction, especially in a single architecture. Here, we report the design of a topology-optimized plasmonic nanoantenna to alleviate the above limitation which could greatly enhance far-field photon extraction. The plasmonic nanoantenna is composed of an optimized gold pattern and a silicon nitride substrate, with a nanohole in the center of the gold pattern. Our design is based on density-based topology optimization and is inherently robust to dimensions and fabrication errors. As a result, the normalized extraction decay rate (γ_e/γ_0) can reach 5.48 at a wavelength of 517 nm if an objective lens with a numerical aperture of 0.45 is utilized. The proposed method to alleviate the contradiction of plasmonic mode volume could brighten the prospects for future integration of single-photon sources into photonic quantum networks and applications in quantum information science.

1. INTRODUCTION

In recent years, quantum information science and technology have been developed by leaps and bounds, and have become the forefront of a new round of scientific and technological revolution and industrial transformation [1–4]. A major challenge in the field of quantum communication is the development of single-photon sources since they are the carrier of quantum information processing, and also the basic resource for realizing quantum technology such as quantum sensing [5–8], quantum communication [9–13], and quantum imaging [14–16]. However, the spontaneous emission rate of quantum emitters in a vacuum is naturally limited to about 1 GHz, which limits the speed of optical devices [17]. Therefore, the photon emission speed-up becomes a major task on the way to implementing high-speed quantum information applications.

The speed-up of the photon emission can be achieved by increasing the density of photon states with the help of nanostructures. According to the Purcell effect [18, 19], nanostructures have been designed to either increase the quality factor or reduce the mode volume to enhance the spontaneous emission decay rate. The realization of large photon emission in dielectric nanostructures (e.g., dielectric micro-cavities) is challenging due to the limitations imposed by diffraction [20]. Although these structures exhibit high-quality factors, this often results in slower operation rates because of the inverse relationship between the quality factor and response time. On the other hand, plasmonic nanostructures are capable of providing highly confined plasmonic modes, which offers a distinct advantage in terms of photon emission [21]. By forming an ultrasmall plasmonic mode volume, plasmonic nanostructures can provide a larger Purcell factor enhancement. This may exceed the diffraction-limited spontaneous emission rate of photons by two orders of magnitude [22–24]. However, plasmonic nanostructures are subject to a typically small quality factor [20] and a limited quantum efficiency [25] due to the significant loss in metals. Thus, these challenges have led to disputes on the optimal choice of platforms for single-photon sources.

In parallel, on-demand single-photon sources with high emission rates can achieve a high repetition rate [1, 26]. This results in higher bit rates in quantum communication and faster readout of stationary qubits [27, 28]. Regarding this matter, plasmonic nanostructures exhibit inherent advantages over dielectric nanostructures. To be specific, the repetition rate is determined by the photon extraction rate of quantum emitters, which is equal to the product of the emitter's spontaneous emission rate and the outcoupling efficiency of excited photons into optics (e.g., microscope) [26]. In other words, the intrinsic far-field photon extraction can be achieved by using, for example, plasmonic nanoantenna and microscope with suitable values of numerical aperture (NA). However, the small mode volume required for emission speed-up and the sufficiently large mode volume required for efficient extraction are always in conflict with each other, resulting in low outcoupling efficiency of quantum emitters into far-field [29].

* Corresponding author: Huaping Wang (hpwang@zju.edu.cn).
# These authors contributed equally to this paper.

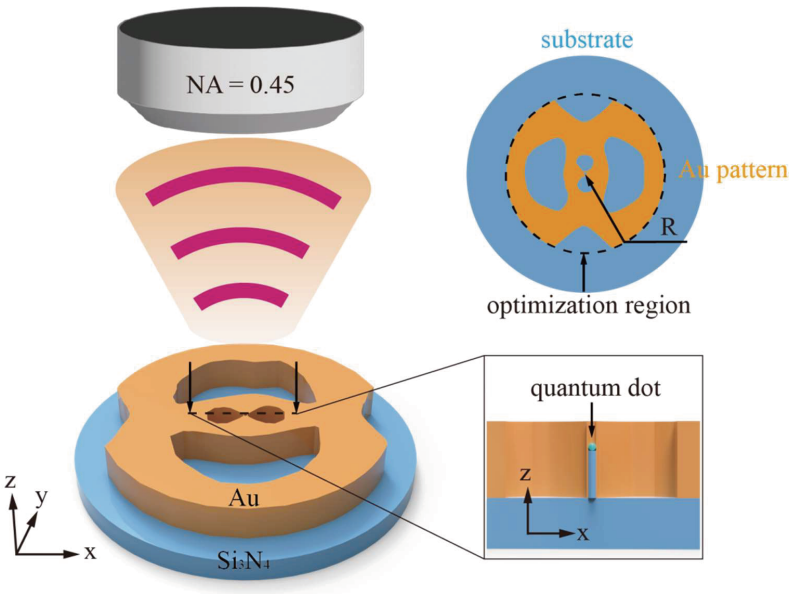

FIGURE 1. Schematic of the plasmonic nanoantenna for single-photon extraction. It consists of an optimized Au pattern and a Si_3N_4 substrate below. An objective lens (NA $= 0.45$, corresponding to a cross-sectional angle 26.7°) is used for the far-field photon extraction. The upper right represents the top view of the plasmonic nanoantenna with a radius (R) of 500 nm. The lower right represents a cross-sectional view of the plasmonic nanoantenna, showing a quantum dot situated within the nanohole.

Thus, the low outcoupling efficiency for far-field photon extraction is the main challenge for practical applications by using plasmonic nanoantenna and optics. Various attempts have been made to improve the far-field photon extraction decay rate in plasmonic nanostructures, such as metallic structures that support gap surface plasmons integrated with phase-matched nanofibers [30], nanopatch antennas [26, 31], and patterned hyperbolic metamaterials [32–35]. However, these attempts are still thought to be less practical or efficient for the realization of single-photon extraction. Recently, topology optimization [36–38] was applied to various inverse design problems for quantum photonic applications. The inverse design optimization frameworks lead to devices with nontrivial shapes and topologies, enabling high performance and compatibility with the predefined fabrication precisions.

In this work, we report the design of a topology-optimized plasmonic nanoantenna to overcome the above intrinsic limitations in plasmonic nanostructures. Inspired by the recent works of topology optimization to realize efficient and coherent light-matter interactions [36–38], we apply a density-based topology optimization framework to optimize the single-photon sources. This work enables far-field photon extraction into optics and gains insight into the physics behind the complex plasmonic nanostructures, leading to emission speed-up and efficient extraction. Specifically, the plasmonic nanoantenna consists of an optimized gold (Au) pattern and a silicon nitride (Si_3N_4) substrate, with a nanohole in the center of the Au pattern (Figure 1). A quantum dot is located inside the nanohole on top of the substrate. The diameter of the quantum dot is exactly equal to the diameter of the nanohole, thus strong field enhancement can be achieved. The collected power is calculated as an integral through a circular area above the emitter, which mimics the emission collection using a commercially available objective lens (NA $= 0.45$, corresponding to a cross-sectional angle 26.7°). As a result, the normalized extraction decay rate (γ_e/γ_0) can reach 5.48 while the Purcell factor is 4200.

2. METHODS AND RESULTS

Numerical modelling is performed using a commercial finite element solver (COMSOL Multiphysics, Wave Optics Module). Topology optimization [36] is used to design the device within a design region situated directly on top of the substrate with a radius of 500 nm. A three-dimensional (3D) schematic diagram of the proposed nanoantenna is shown in Figure 1. A CdSe/ZnS core-shell quantum dot (PL peak 517 nm and $\varepsilon_{ZnS} = 5.81$) [39] is placed inside the central nanohole of the Au pattern, sharing the same diameter ($d = 12$ nm) as the quantum dot. To facilitate the placement of quantum dots, Si_3N_4 is adopted as the substrate below as shown in Figure 1, $\varepsilon_{Si_3N_4} = 4.12$. The dielectric constant of Au can be taken from the experimental data [40]. To estimate the photon emission and extraction of quantum dots, the following assumption is applied. First, we assume that the light-matter interaction inside plasmonic nanoantenna works in the weak-coupling regime [41], that means the non-radiative damping of single-photon sources is larger than the interaction strength between the quantum dots and the plasmonic nanoantenna. Thus, the outcomes are in good agreement with the treatment of classical electrodynamics principles [42]. Second, the quantum dot considered in this work is simulated as an oscillating classical point dipole inside a dielectric host with a polarization direction parallel to the x-direction. Due to the high photonic density of states generated by the plasmonic nanoantenna, the quantum dot exhibits a large spontaneous emission.

The objective of the topology optimization is to enhance the far-field photon extraction γ_e through an objective lens (NA

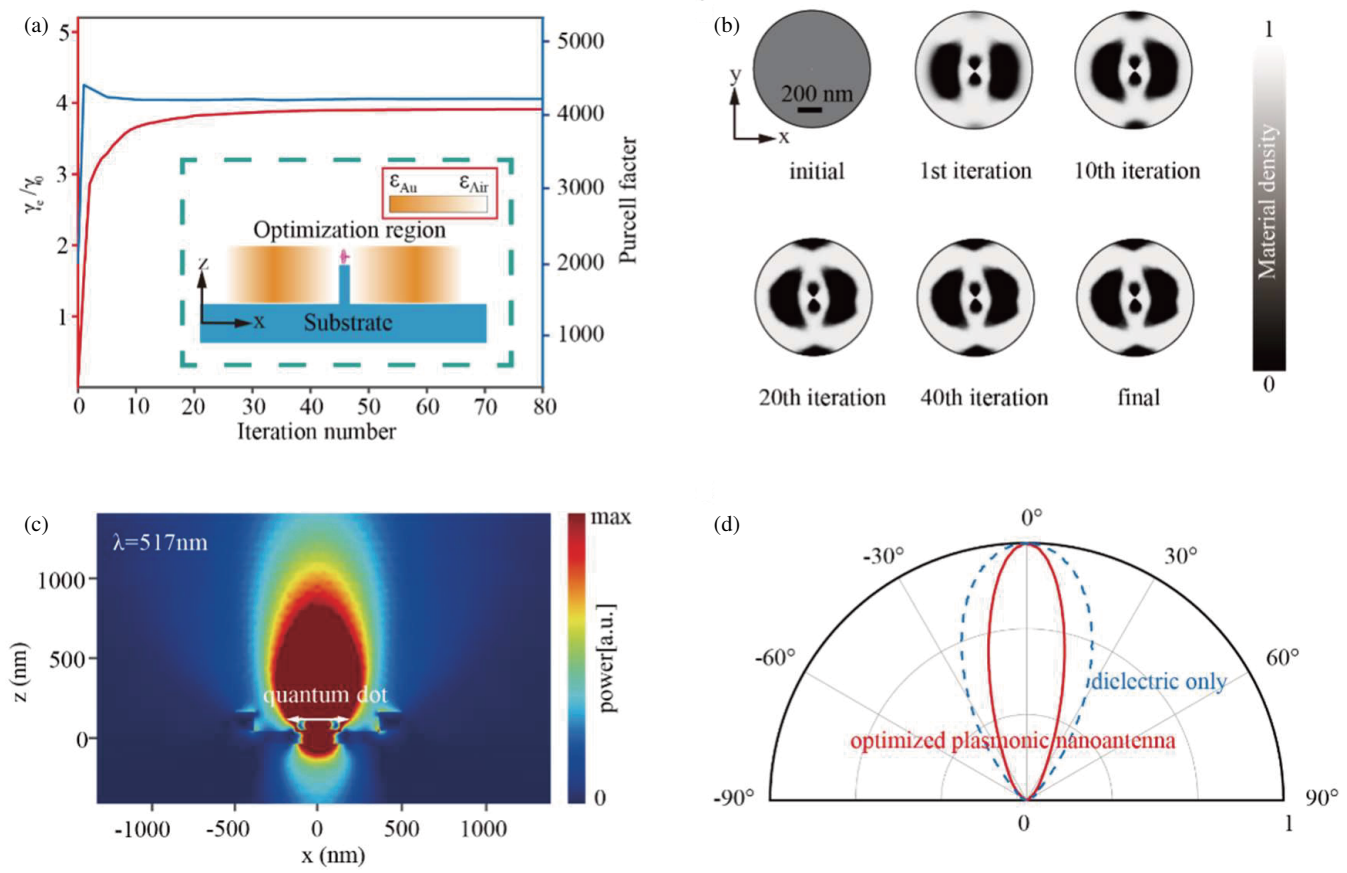

FIGURE 2. Topology optimization for the plasmonic nanoantenna. (a) Normalized extraction decay rate γ_e/γ_0 (red) as a function of the iteration number for a full three-dimensional optimization run. The working wavelength of λ= 517 nm is chosen for illustration, since it is the radiation spectrum of CdSe/ZnS core-shell quantum dots which is within the blue-green spectral range. The Purcell factor (blue) versus the iteration number is also shown here. (b) Corresponding evolution of the material density distribution within the optimization region. (c) Power density distribution in the xOz plane under the coupling of quantum dots and optimized plasmonic nanoantenna. (d) The angular pattern. The case for a nanostructure with dielectric only is also calculated for comparison.

$= 0.45$) with a radius of 500 nm, which is located 992 nm above the plasmonic nanoantenna. The thicknesses of Au pattern and Si_3N_4 substrate are 120 nm and 80 nm, respectively Performing surface integration at the surface of the objective lens, the power of the photon extraction into the objective lens can be obtained, $W_e = \iint_F S \cdot \hat{z} dxdy$. The normalized extraction decay rates can be obtained from $\gamma_e/\gamma_0 = W_e/W_0$, where γ_e is the extraction decay rate. γ_0 and W_0 are the spontaneous emission rate and the total radiated power of a quantum emitter in vacuum, respectively. In addition, the quantum emitter in a plasmonic nanoantenna will experience an enhanced radiation rate relative to that in a homogenous medium given by the Purcell factor [17], F_P=$\gamma_{\text{total}}/\gamma_0 = W_{\text{total}}/W_0$, where γ_{total} means the total photon emission rate, and the total emitted power W_{total} of the quantum emitter can be numerically computed as the integral of power flux through a spherical surface with a radius of 2 nm centered on the point dipole.

Initially, the material distribution in the optimization domain is set to be a smooth distribution with the following permittivity function

$$\varepsilon(x,y) = \varepsilon_{\text{Air}}[1-\rho(x,y)] + \varepsilon_{\text{Au}}\rho(x,y), \quad \rho \in [0,1] \qquad (1)$$

where $\rho(x,y)$ is the material density distribution that varies from 0 (air) to 1 (Au); ε_{Air} and ε_{Au} are the dielectric constants of the air and Au, respectively. In principle, topology optimization allows the relative dielectric constant of each discrete voxel in the design area to be one degree of freedom, and the actual degrees of freedom form a two-dimensional (2D) grid. To design a nanostructure that can be practically manufactured using top-down techniques, it is crucial to maintain a consistent configuration in the z-direction. The optimized distribution of 2D materials stretches along the z-direction, leading to the creation of a topology-optimized plasmonic nanoantenna.

3. DISCUSSION

Figure 2(a) shows the optimization process of far-field photon extraction, which tends to saturate near the steady-state local solution. The working wavelength of $\lambda = 517$ nm is chosen for illustration since it is the radiation spectrum of CdSe/ZnS core-shell quantum dots which is within the blue-green spectral range [43]. The optimization starts with an initial material distribution of $\rho(x,y) = 0.5$ and gradually converges to the binary material mode at the end of the optimization cycle

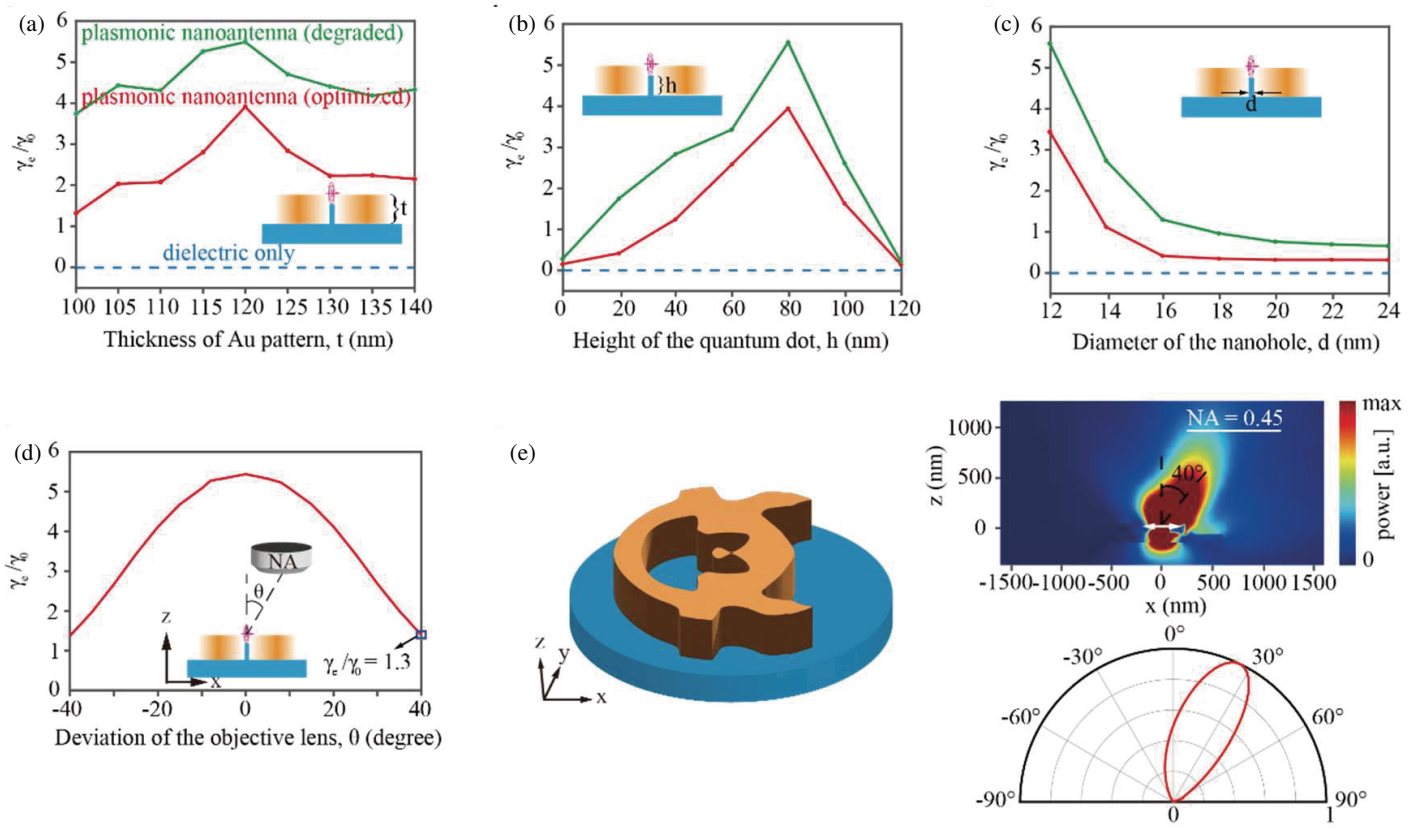

FIGURE 3. The influence of emitters on radiation intensity and directionality. Normalized extraction decay rates γ_e/γ_0 versus (a) thickness of Au pattern, (b) height of the quantum dot and (c) diameter of the quantum dot. The working wavelength of λ= 517 nm is chosen for illustration. Both degraded and optimized cases for plasmonic nanoantennas are shown here. Moreover, the cases for nanostructures with dielectric only are also shown for comparison. (d) Normalized extraction decay rate γ_e/γ_0 when the objective lens is deviated. The deviation angle is shown in the inset. (e) Optimized plasmonic nanoantenna when the deviation angle is $\theta = 40°$. The basic setup is the same as Figure 2. The power density distribution as well as the angular pattern are also shown here.

(Figure 2(b)). During the optimization process, the photon extraction increases, and when the optimization reaches its termination criteria, the performance has already become stable. Subsequent continuation of the optimization process no longer yields significant improvement in the normalized extraction decay rates. Because achieving a fully binarized distribution without extreme binarization coefficients may require a significant amount of iterations, with almost no change in repeated calculations for the same structure. To shorten the optimization time, once the ratio of the number of voxels in air/Au to all voxels reaches the required threshold (binarization >80%), the optimization stops. At this point, the material density matrix is completely binarized by thresholding all the voxels and forcing them to take a binary value, a process known as degradation [44]. Therefore, the optimized nanoantenna can be obtained when the optimization is stopped and then the degraded nanoantenna can be obtained after performing thresholding operation to achieve full binarization (Figures 3(a)–(c)). During the topology optimization process, along with the enhancement of normalized extraction decay rate that reaches 5.48, the Purcell factor of the nanoantenna can also increase to 4200. Correspondingly, we find significant radiation fields being extracted into the objective lens in Figure 2(c). The simulated results show that the normalized extraction decay rate is about 280 times larger than the one in nanostructure with dielectric only ($\gamma_e/\gamma_0 \approx 0.019$). To characterize radiation directionality, the corresponding angular patterns to retrieve 2D angular far-field emission patterns are plotted in Figure 2(d). It is shown that the plasmonic nanoantenna could improve the radiation directionality to a certain extent.

One should note that during the optimization process, the thickness of the Au pattern, the height of the quantum dot inside the nanohole as well as the diameter of the nanohole are preselected. To find the ideal thickness of the Au pattern, we perform a series of topology optimizations for a thickness range from 100 nm to 140 nm (Figure 3(a)). We find that the optimized (before degradation) and degraded results within the range are optimal at a thickness of approximately 120 nm. In addition, due to the limited accuracy of point defect localization, the design should have robustness to resist the uncertainty of the quantum dot's position within the nanoantenna. Although the optimized plasmonic nanoantenna is based on a fixed quantum dot with a height of 80 nm, we also simulate its performance at different heights (Figure 3(b)). When the nanohole contains no dielectric material, the quantum dot is placed directly on the substrate, resulting in an approximate height of zero ($h = 0$ nm). This

configuration significantly reduces the normalized extraction decay rates. Obviously, the normalized extraction decay rate increases with the increase in height, and at a height of 80 nm, it reaches the optimal value.

On the other hand, it is reasonable to expect that the manufacturing process will lead to deviations in edge positions. Due to the placement of quantum dots inside the central nanohole, the size of the nanohole is small, resulting in machining errors. To facilitate the placement of a quantum dot, the diameter of the nanohole needs to be larger than that of the quantum dot. Figure 3(c) shows the effect of increasing the diameter of the nanohole on the extraction decay rates. Due to the near-field coupling, we could find that the smaller the nanohole is, the better the performance of the plasmonic nanoantenna could be obtained. For far-field photon extraction, it is better to position the objective lens vertically above the nanoantenna. However, due to the positioning technique for the objective lens, the angular deviation might occur during the extraction process. We show that the optimized plasmonic nanoantenna still maintains good performance within the extraction offset range of $-40°$ to $40°$ (Figure 3(d)). We find that when the extraction surface is offset by $\pm 40°$, the normalized extraction decay rate is about 1.3. To verify the effectiveness of the topology optimization process, we do the optimization in the case where the deviation angle is $40°$ (Figure 3(e)). Correspondingly, we find significant radiation fields being extracted into the objective lens with a deviation angle of $40°$. Since the radius of the objective lens is 500 nm, it is possible to extract photons from an angle range of $18.5°$ to $53.3°$. Therefore, we find that the maximum directional angle for far-field photon extraction is less than $40°$ from the angular pattern. Nevertheless, we could realize efficient photon extraction ($\gamma_e/\gamma_0 = 2.5$) if the objective lens deviates with an angle of $40°$, which is nearly twice as much as the original one.

4. CONCLUSION

In summary, we have designed a plasmonic nanoantenna based on a density-based topology optimization framework. Through a systematic study of the plasmonic nanoantenna based on topology optimization, we have demonstrated their strong ability to alleviate the contradiction of plasmonic mode volume and enhance far-field photon extraction into optics. We could find that the proposed plasmonic nanoantenna functions like a combination of the bowtie antenna [45] and bullseye antenna [46], which could comprehensively improve the photon extraction of a quantum dot positioning inside the nanohole. By leveraging the design flexibility offered by topology optimization, our method effectively capitalizes on the strengths while avoiding the weaknesses of conventional plasmonic and dielectric nanostructures. Overall, the optimized plasmonic nanoantenna could realize a normalized extraction decay rate of 5.48 with the Purcell factor reaching 4200. More prominently, the proposed plasmonic nanoantenna as well as topology optimization could be readily extended to other research domains of optics and materials science, enabling on-demand single-photon sources into photonic quantum networks and applications in quantum information science.

DATA AVAILABILITY

The data that supports the findings of this study are available within the article.

ACKNOWLEDGEMENT

The work was sponsored by the National Natural Science Foundation of China (NNSFC) under Grants No. 61905216, 62275231, 61975176, 62175212, Key Research and Development Program of the Ministry of Science and Technology under Grants No. 2022YFA1404704, 2022YFA1405200, and 2022YFA1404902, Zhejiang Provincial Natural Science Fund Key Project under Grant No. LZ23F050003, the Key Research and Development Program of Zhejiang Province under Grant No. 2022C01036, Natural Science Foundation of Ningbo under Grant No. 2021J152, and the Fundamental Research Funds for the Central Universities (2021FZZX001-19).

REFERENCES

[1] O'brien, J. L., A. Furusawa, and J. Vučković, "Photonic quantum technologies," *Nature Photonics*, Vol. 3, No. 12, 687–695, 2009.

[2] Loss, D. and D. P. DiVincenzo, "Quantum computation with quantum dots," *Physical Review A*, Vol. 57, No. 1, 120, 1998.

[3] Liu, X. and M. C. Hersam, "2D materials for quantum information science," *Nature Reviews Materials*, Vol. 4, No. 10, 669–684, 2019.

[4] Yuan, H. Y., Y. Cao, A. Kamra, R. A. Duine, and P. Yan, "Quantum magnonics: When magnon spintronics meets quantum information science," *Physics Reports*, Vol. 965, 1–74, 2022.

[5] Degen, C. L., F. Reinhard, and P. Cappellaro, "Quantum sensing," *Reviews of Modern Physics*, Vol. 89, No. 3, 035002, 2017.

[6] Boss, J. M., K. S. Cujia, J. Zopes, and C. L. Degen, "Quantum sensing with arbitrary frequency resolution," *Science*, Vol. 356, No. 6340, 837–840, 2017.

[7] Schmitt, S., T. Gefen, F. M. Stürner, *et al.*, "Submillihertz magnetic spectroscopy performed with a nanoscale quantum sensor," *Science*, Vol. 356, No. 6340, 832–837, 2017.

[8] Pirandola, S., B. R. Bardhan, T. Gehring, C. Weedbrook, and S. Lloyd, "Advances in photonic quantum sensing," *Nature Photonics*, Vol. 12, No. 12, 724–733, 2018.

[9] Chen, Y.-A., Q. Zhang, T.-Y. Chen, W.-Q. Cai, S.-K. Liao, J. Zhang, K. Chen, J. Yin, J.-G. Ren, Z. Chen, *et al.*, "An integrated space-to-ground quantum communication network over 4,600 kilometres," *Nature*, Vol. 589, No. 7841, 214–219, 2021.

[10] Sidhu, J. S., S. K. Joshi, M. Gündoğan, *et al.*, "Advances in space quantum communications," *IET Quantum Communication*, Vol. 2, No. 4, 182–217, 2021.

[11] Couteau, C., S. Barz, T. Durt, T. Gerrits, J. Huwer, R. Prevedel, J. Rarity, A. Shields, and G. Weihs, "Applications of single photons to quantum communication and computing," *Nature Reviews Physics*, Vol. 5, No. 6, 326–338, 2023.

[12] Vajner, D. A., L. Rickert, T. Gao, K. Kaymazlar, and T. Heindel, "Quantum communication using semiconductor quantum dots," *Advanced Quantum Technologies*, Vol. 5, No. 7, 2100116, 2022.

[13] Pirandola, S., R. Laurenza, C. Ottaviani, and L. Banchi, "Fundamental limits of repeaterless quantum communications," *Nature Communications*, Vol. 8, No. 1, 1–15, 2017.

[14] Gilaberte Basset, M., F. Setzpfandt, F. Steinlechner, E. Beckert, T. Pertsch, and M. Gräfe, "Perspectives for applications of quantum imaging," *Laser & Photonics Reviews*, Vol. 13, No. 10,

1900097, 2019.

[15] Brida, G., M. Genovese, and I. R. Berchera, "Experimental realization of sub-shot-noise quantum imaging," *Nature Photonics*, Vol. 4, No. 4, 227–230, 2010.

[16] Taylor, M. A., J. Janousek, V. Daria, J. Knittel, B. Hage, H.-A. Bachor, and W. P. Bowen, "Subdiffraction-limited quantum imaging within a living cell," *Physical Review X*, Vol. 4, No. 1, 011017, 2014.

[17] Bogdanov, S. I., A. Boltasseva, and V. M. Shalaev, "Overcoming quantum decoherence with plasmonics," *Science*, Vol. 364, No. 6440, 532–533, 2019.

[18] Agio, M. and D. M. Cano, "The Purcell factor of nanoresonators," *Nature Photonics*, Vol. 7, No. 9, 674–675, 2013.

[19] Cang, H., Y. Liu, Y. Wang, X. Yin, and X. Zhang, "Giant suppression of photobleaching for single molecule detection via the Purcell effect," *Nano Letters*, Vol. 13, No. 12, 5949–5953, 2013.

[20] Bozhevolnyi, S. I. and J. B. Khurgin, "Fundamental limitations in spontaneous emission rate of single-photon sources," *Optica*, Vol. 3, No. 12, 1418–1421, 2016.

[21] Tame, M. S., K. R. McEnery, □. K. Özdemir, J. Lee, S. A. Maier, and M. S. Kim, "Quantum plasmonics," *Nature Physics*, Vol. 9, No. 6, 329–340, 2013.

[22] Zhou, Z.-K., J. Liu, Y. Bao, L. Wu, C. E. Png, X.-H. Wang, and C.-W. Qiu, "Quantum plasmonics get applied," *Progress in Quantum Electronics*, Vol. 65, 1–20, 2019.

[23] Russell, K. J., T.-L. Liu, S. Cui, and E. L. Hu, "Large spontaneous emission enhancement in plasmonic nanocavities," *Nature Photonics*, Vol. 6, No. 7, 459–462, 2012.

[24] Akselrod, G. M., C. Argyropoulos, T. B. Hoang, C. Ciracì, C. Fang, J. Huang, D. R. Smith, and M. H. Mikkelsen, "Probing the mechanisms of large Purcell enhancement in plasmonic nanoantennas," *Nature Photonics*, Vol. 8, No. 11, 835–840, 2014.

[25] Işiklar, G., P. T. Kristensen, J. Mørk, O. Sigmund, and R. E. Christiansen, "On the trade-off between mode volume and quality factor in dielectric nanocavities optimized for Purcell enhancement," *Optics Express*, Vol. 30, No. 26, 47 304–47 314, 2022.

[26] Yang, G., Q. Shen, Y. Niu, H. Wei, B. Bai, M. H. Mikkelsen, and H.-B. Sun, "Unidirectional, ultrafast, and bright spontaneous emission source enabled by a hybrid plasmonic nanoantenna," *Laser & Photonics Reviews*, Vol. 14, No. 3, 1900213, 2020.

[27] Neumann, P., J. Beck, M. Steiner, F. Rempp, H. Fedder, P. R. Hemmer, J. Wrachtrup, and F. Jelezko, "Single-shot readout of a single nuclear spin," *Science*, Vol. 329, No. 5991, 542–544, 2010.

[28] Dutt, M. V. G., L. Childress, L. Jiang, E. Togan, J. Maze, F. Jelezko, A. S. Zibrov, P. R. Hemmer, and M. D. Lukin, "Quantum register based on individual electronic and nuclear spin qubits in diamond," *Science*, Vol. 316, No. 5829, 1312–1316, 2007.

[29] Bogdanov, S. I., O. A. Makarova, X. Xu, Z. O. Martin, A. S. Lagutchev, M. Olinde, D. Shah, S. N. Chowdhury, A. R. Gabidullin, I. A. Ryzhikov, *et al.*, "Ultrafast quantum photonics enabled by coupling plasmonic nanocavities to strongly radiative antennas," *Optica*, Vol. 7, No. 5, 463–469, 2020.

[30] Sugawara, M., Y. Xuan, Y. Mitsumori, K. Edamatsu, and M. Sadgrove, "Plasmon-enhanced single photon source directly coupled to an optical fiber," *Physical Review Research*, Vol. 4, No. 4, 043146, 2022.

[31] Bogdanov, S. I., M. Y. Shalaginov, A. S. Lagutchev, C.-C. Chiang, D. Shah, A. S. Baburin, I. A. Ryzhikov, I. A. Rodionov, A. V. Kildishev, A. Boltasseva, and V. M. Shalaev, "Ultrabright room-temperature sub-nanosecond emission from single nitrogen-vacancy centers coupled to nanopatch antennas," *Nano Letters*, Vol. 18, No. 8, 4837–4844, 2018.

[32] Galfsky, T., H. N. S. Krishnamoorthy, W. Newman, E. E. Narimanov, Z. Jacob, and V. M. Menon, "Active hyperbolic metamaterials: Enhanced spontaneous emission and light extraction," *Optica*, Vol. 2, No. 1, 62–65, 2015.

[33] Lu, D., J. J. Kan, E. E. Fullerton, and Z. Liu, "Enhancing spontaneous emission rates of molecules using nanopatterned multilayer hyperbolic metamaterials," *Nature Nanotechnology*, Vol. 9, No. 1, 48–53, 2014.

[34] Shen, L., X. Lin, M. Y. Shalaginov, T. Low, X. Zhang, B. Zhang, and H. Chen, "Broadband enhancement of on-chip single-photon extraction via tilted hyperbolic metamaterials," *Applied Physics Reviews*, Vol. 7, No. 2, 021403, 2020.

[35] Qin, Z., L. Shen, M. Shalaginov, H. Wang, H. Chen, and X. Lin, "Single-photon extraction via spatial topological transition," *Applied Physics Reviews*, Vol. 11, No. 1, 011412, 2024.

[36] Jensen, J. S. and O. Sigmund, "Topology optimization for nano-photonics," *Laser & Photonics Reviews*, Vol. 5, No. 2, 308–321, 2011.

[37] Wambold, R. A., Z. Yu, Y. Xiao, B. Bachman, G. Jaffe, S. Kolkowitz, J. T. Choy, M. A. Eriksson, R. J. Hamers, and M. A. Kats, "Adjoint-optimized nanoscale light extractor for nitrogen-vacancy centers in diamond," *Nanophotonics*, Vol. 10, No. 1, 393–401, 2020.

[38] Yesilyurt, O., Z. A. Kudyshev, A. Boltasseva, V. M. Shalaev, and A. V. Kildishev, "Efficient topology-optimized couplers for on-chip single-photon sources," *ACS Photonics*, Vol. 8, No. 10, 3061–3068, 2021.

[39] Fu, Y., D. Kim, W. Jiang, W. Yin, T. K. Ahn, and H. Chae, "Excellent stability of thicker shell CdSe@ ZnS/ZnS quantum dots," *RSC Advances*, Vol. 7, No. 65, 40 866–40 872, 2017.

[40] Johnson, P. B. and R. W. Christy, "Optical constants of the noble metals," *Physical Review B*, Vol. 6, No. 12, 4370, 1972.

[41] Shalaginov, M. Y., V. V. Vorobyov, J. Liu, M. Ferrera, A. V. Akimov, A. Lagutchev, A. N. Smolyaninov, V. V. Klimov, J. Irudayaraj, A. V. Kildishev, and e. al., "Enhancement of single-photon emission from nitrogen-vacancy centers with TiN/(Al, Sc) N hyperbolic metamaterial," *Laser & Photonics Reviews*, Vol. 9, No. 1, 120–127, 2015.

[42] Yeung, M. S. and T. K. Gustafson, "Spontaneous emission near an absorbing dielectric surface," *Physical Review A*, Vol. 54, No. 6, 5227, 1996.

[43] Ji, L., J. Gao, A.-L. Yang, Z. Feng, X.-F. Lin, Z.-G. Li, and X.-M. Jin, "Towards quantum communications in free-space seawater," *Optics Express*, Vol. 25, No. 17, 19 795–19 806, 2017.

[44] Chakravarthi, S., P. Chao, C. Pederson, S. Molesky, A. Ivanov, K. Hestroffer, F. Hatami, A. W. Rodriguez, and K.-M. C. Fu, "Inverse-designed photon extractors for optically addressable defect qubits," *Optica*, Vol. 7, No. 12, 1805–1811, 2020.

[45] Kinkhabwala, A., Z. Yu, S. Fan, Y. Avlasevich, K. Müllen, and W. E. Moerner, "Large single-molecule fluorescence enhancements produced by a bowtie nanoantenna," *Nature Photonics*, Vol. 3, No. 11, 654–657, 2009.

[46] Andersen, S. K. H., S. Bogdanov, O. Makarova, Y. Xuan, M. Y. Shalaginov, A. Boltasseva, S. I. Bozhevolnyi, and V. M. Shalaev, "Hybrid plasmonic bullseye antennas for efficient photon collection," *ACS Photonics*, Vol. 5, No. 3, 692–698, 2018.